MNRAS **000**, 1–?? (2017) Preprint 21 April 2017 Compiled using MNRAS LATEX style file v3.0

The SAMI Galaxy Survey: Quenching star formation in GAMA groups

A. L. Schaefer[1,2,3], S. M. Croom[1,3], N. Scott[1,3], S. Brough[3,4], J. T. Allen[1,2], J. Bland-Hawthorn[1], J. V. Bloom[1,3], J. J. Bryant[1,2,3], C. Federrath[5], L. M. R. Fogarty[1], A. M. Hopkins[2], I. S. Konstantopoulos[2,6], A. R. López-Sánchez[2,7], J. S. Lawrence[2], A. M. Medling[5,8], M. S. Owers[3,7], S. N. Richards[1,2,3], A. S. G. Robotham[9], S. K. Yi[10], J. van de Sande[1]

[1] *Sydney Institute for Astronomy, School of Physics, University of Sydney, NSW 2006, Australia*
[2] *Australian Astronomical Observatory (AAO), PO Box 915, North Ryde, NSW 1670, Australia*
[3] *CAASTRO: ARC Centre of Excellence for All-sky Astrophysics*
[4] *School of Physics, University of New South Wales, NSW 2052, Australia*
[5] *Research School of Astronomy and Astrophysics, Australian National University, Canberra, ACT 2611, Australia*
[6] *Atlassian 341 George St Sydney, NSW 2000*
[7] *Department of Physics and Astronomy, Macquarie University, NSW 2109, Australia*
[8] *Cahill Center for Astronomy and Astrophysics, California Institute of Technology, MS 249-17 Pasadena, CA 91125, USA*
[9] *SUPA School of Physics & Astronomy, University of St Andrews KY16 9SS Scotland*
[10] *Department of Astronomy and Yonsei University Observatory, Yonsei University, Seoul 03722, Republic of Korea*

2017

ABSTRACT

We explore the radial distribution of star formation in galaxies in the Sydney Australian Astronomical Observatory Multi-object Integral Field Spectrograph (SAMI) as a function of their local group environment, and other measures of environment associated with the suspected mechanisms for environmental quenching. We find that the dynamical mass of the parent halo of a galaxy is a good predictor of environmental quenching. Higher mass group environments reduce the specific star formation rates of galaxies, but the spatially-resolved signature of this reduction appears to vary with the stellar mass of each galaxy. Galaxies more massive than $M_* \sim 10^{10}\,M_\odot$ have star formation quenched first in their outskirts, while galaxies less massive than this appear to be quenched uniformly across their discs. The dominant star-forming galaxies in groups with mass less than $10^{12.5}\,M_\odot$ appear to have their star formation enhanced by $\sim 0.2 \pm 0.09$ dex over non-group galaxies of the same mass, with weak evidence that this enhancement occurs in the centres of these galaxies.

1 INTRODUCTION

Much of the literature on the impact of galaxy environments on their star formation has been confined to studies of galaxy clusters. In these environments the evidence suggests that the removal of gas from galaxies and subsequent suppression of star formation is likely to be caused by one of two primary mechanisms: Ram pressure stripping or strangulation. Ram pressure stripping occurs when the kinetic interaction between the interstellar medium (ISM) of a galaxy in the intergalactic medium (IGM) forces the gas out of the galaxy (Gunn & Gott 1972). Strangulation occurs when the infall of gas onto the disc of a galaxy is halted, starving the galaxy of fuel for future star formation (Larson, Tinsley, & Caldwell 1980). Strangulation has also been proposed as one of the primary mechanisms for star formation quenching outside of clusters (Peng, Maiolino, & Cochrane 2015). Narrow-band imaging studies of the distribution of Hα emission in Virgo cluster galaxies (e.g. Koopmann & Kenney 2004a,b; Koopmann, Haynes, & Catinella 2006) indicate that the ram pressure stripping of gas from galaxy discs is the main mechanism acting to suppress star formation. This conclusion is backed up by Cortese et al. (2012), who showed that the relative spatial extent of ultraviolet emission in Virgo galaxies was correlated with the amount of neutral gas present. In contrast to these results, other works that examined different star formation rate indicators as a function of environment density (e.g. von der Linden et al. 2010) derived a slower quenching timescale, suggesting quenching takes place over several Gyr and implying that ram pressure stripping can not be the primary physical mechanism.

Although clusters represent the most extreme environments, only approximately 5% of galaxies exist in rich clusters. There is evidence that less extreme environments such as galaxy groups play a role in quenching star formation in galaxies in the local universe. Since approximately $40-50\%$ of galaxies exist in groups at $z \sim 0$ (Eke et al. 2004;

Robotham et al. 2011), the majority of environment-driven galaxy evolution is likely to occur outside of clusters.

For example, Wilman et al. (2005) showed a strong decline in the number of emission-line galaxies in groups between $z = 0.5$ and the present day. This work, and many other studies of large samples derived from spectroscopic and photometric surveys, have reached the conclusion that the environmental quenching of star formation must be a rapid process (Balogh et al. 2004; Wijesinghe et al. 2011). In these studies the scarcity of galaxies in transition between star-forming and passive was interpreted to signify a rapid quenching timescale. However, the measurement of the integrated star formation rates of galaxies from central spectra or integrated colours is not without its perils. Schawinski et al. (2014) cautioned that the interpretation of the rarity of galaxies between the star-forming blue cloud and the passive red sequence as rapid quenching is erroneous if galaxy morphology is not taken into account.

In a study that made a robust, multi-wavelength comparison of twelve different star formation rate metrics, Davies et al. (2016b) showed that the star formation rate calibrations can vary markedly between surveys. Differences between the star formation rates of populations of galaxies derived by different means can make direct comparisons of the quenching timescales found by different authors problematic. Further, aperture biases are a concern for single-fibre spectroscopy and thus the quenching timescales in dense environments have remained controversial.

Other authors, using data from single-fibre spectroscopic surveys, have argued that much of the environment-driven evolution of galaxies can be explained by interactions between close pairs. Robotham et al. (2014) showed that galaxies that are both dynamically and spatially close to their nearest neighbour are likely to have disturbed optical morphologies. This idea was expanded upon by Davies et al. (2015), who showed that separations between galaxies in pairs of less than ~ 30 kpc. Their data showed that for galaxies in close pairs, the more massive galaxy tended to have its star formation enhanced, while the less massive galaxy had its star formation suppressed. They posited that the tidal disturbance of gas in the more massive galaxy would trigger star-formation. While the enhancement of star formation in close pairs was also reported in other studies (e.g. Patton et al. 2013), they did not study the suppression of star formation during these interactions. Davies et al. (2016a) showed that galaxies with stellar masses below $\sim 10^{8.5}\,\mathrm{M}_{\odot}$ become quiescent only in the presence of a more massive companion and argued that the increasing timescales for interaction between a galaxy of this mass and a more massive companion are consistent with their star formation being suppressed by strangulation. It is unclear whether the the environmental suppression of star formation in groups is due to galaxy-galaxy interactions or whether it can be attributed to the impact of the group environment at large.

Rasmussen et al. (2012) observed the star formation rates of star-forming galaxies in groups to be suppressed by 40 per cent relative to galaxies outside of groups and that this environmental quenching is visible out to $\sim 2\mathrm{r}_{200}$. Their analysis of the distribution of star-forming galaxies in groups implied that star formation is quenched in galaxies on timescales of approximately 2 Gyr and is accomplished by a combination of ram pressure stripping and galaxy-galaxy interactions.

This conclusion is backed up by results from the narrow-band Hα Galaxy Group Imaging Survey (HAGGIS; Kulkarni 2015)[1]. By examining the detailed distributions of Hα emission in galaxies in groups, they observed that galaxies below the star formation rate main sequence typically had compact star formation with a steep radial profile. They also noted that differences in the distribution of stellar light for galaxies that are apparently in the process of quenching compared to main-sequence systems implicate some kind of gravitational interaction in the evolution of these systems.

The evidence that ram pressure stripping plays a role in the suppression of star formation in galaxy groups is mounting. Brown et al. (2017) observed that the neutral gas in group galaxies is reduced relative to isolated galaxies, and that this was most strongly correlated with the group halo mass rather than the local galaxy density. A comparison of their results to semi-analytic models and hydrodynamic simulations showed that ram pressure stripping was required to reproduce the observations. While these observations are analogous to other work done in studies of galaxy clusters (e.g. Cortese et al. 2012; Fossati et al. 2013), this was the first time such data has been able to show that ram pressure stripping is a major factor in the evolution of galaxies in groups.

Schaefer et al. (2017) showed that as the local environment density increases around a galaxy, the specific star formation rates (sSFR; SFR/M_{*}) drop and this reduction in star formation occurs in the outer parts of the galaxy. The steepening of the radial profiles of star formation in the densest environments in the sample were not accompanied by a significant change in the central star formation rate surface density, and they concluded that quenching occurs from the outside-in in the environments they studied. In this paper we follow on from the results of Schaefer et al. (2017), studying how the spatial distribution of star formation changes in galaxies relative to physically motivated measures of local environment, in particular the properties of their local groups, their location within those groups and the estimated tidal force acting on each galaxy. Our current work assumes a flat ΛCDM cosmology with $H_0 = 70$ km s^{-1} Mpc^{-1}, $\Omega_M = 0.27$ and $\Omega_\Lambda = 0.73$. Unless otherwise stated, we adopt a Chabrier (2003) stellar initial mass function for calculations of star formation rates.

2 METHODS

2.1 SAMI Data

The data for this study have been taken from the Sydney-Australian Astronomical Observatory Multi-object Integral Field Spectrograph (SAMI; Croom et al. 2012) Galaxy Survey and the Galaxy and Mass Assembly (GAMA; Driver et al. 2011; Hopkins et al. 2013) survey. The SAMI Galaxy Survey is an ongoing resolved spectroscopic survey of approximately 3600 galaxies performed using SAMI, which is mounted on the 3.9 m Anglo-Australian Telescope (AAT) at

[1] Accessible at: https://edoc.ub.uni-muenchen.de/18818/1/Kulkarni_Sandesh.pdf

Siding Spring Observatory in Australia. SAMI comprises 13 optical fibre hexabundles plugged into a steel plate at the prime focus of the AAT, 12 of which are used to observe galaxies while the remaining hexabundle observes a standard star. These optical fibres feed into the AAOmega spectrograph, where the light is split into a red arm ($\lambda\lambda 6300 - 7400$ Å) and dispersed at a resolution of $R = 4260$, and a blue arm ($\lambda\lambda 3700 - 5800$ Å) where it is dispersed to a resolution of $R = 1810$ (van de Sande et al. 2017). The SAMI hexabundles are made of 61 optical fibres fused to cover an approximately circular field of view with a 15″ diameter on the sky. Within each hexabundle the optical fibres fill the aperture with an efficiency of $\sim 73\%$. As a result, observations of galaxies with SAMI must be dithered to uniformly cover the image. We used approximately 7 pointings of 1800 s integrations for a total 12600 s exposure. The raw data are reduced using the SAMI data reduction package, which has been written in the PYTHON language[2] and makes use of the 2dFDR pipeline (Croom, Saunders, & Heald 2004). The circular fibre cores are resampled onto a regular grid of 50×50 0.″5 spaxels. For a full description of the data reduction, see Allen et al. (2015) and for a discussion of representing the fibre data in a regularly gridded data cube see Sharp et al. (2015).

The galaxies observed for the main SAMI Galaxy Survey sample have been drawn from the equatorial regions of the GAMA spectroscopic survey (see Section 2.2). The SAMI survey sample has a stepped selection function in stellar mass with redshift such that the final sample has a nearly uniform distribution of stellar masses. This sample selection covers a wide range of galaxy stellar masses ($10^7 < M_*/M_\odot < 10^{11.5}$) in the redshift range $0.004 < z < 0.11$ and includes galaxies in a wide variety of environments from non-group galaxies to galaxies in 10^{14} $M_\odot$ group halos. The SAMI survey augments the main GAMA-selected sample with a targeted sample of ~ 900 cluster galaxies (Owers et al. 2017), chosen from the 2 Degree Field Galaxy Redshift Survey (Colless et al. 2001) and the Sloan Digital Sky Survey (York et al. 2000; Abazajian et al. 2009). The cluster galaxies have not been used for this work. A thorough discussion of the SAMI target selection is given in Bryant et al. (2015).

2.2 GAMA Data

GAMA, the parent survey for SAMI, is a deep, highly complete spectroscopic survey of galaxies made in three equatorial regions centred on 9, 12 and 15 hours Right Ascension, with additional non-equatorial fields that were not used for the SAMI selection. The equatorial fields have 98.5% complete spectroscopy to $r = 19.8$ mag, two magnitudes deeper than the SDSS (Liske et al. 2015).

2.2.1 Sérsic photometry

The GAMA survey targeted regions that have been covered by SDSS imaging in the u, g, r, i and z photometric bands. These images were re-analysed by Kelvin et al. (2012), who extracted objects from the images and fit single component Sérsic profiles to galaxies. We have made use of these data products, in particular the measurements of the effective radii (r_e), ellipticities and position angles extracted from the Sérsic fits to the SDSS r-band images.

2.2.2 Stellar Masses

We have used the GAMA estimates of the stellar masses of the galaxies in our sample and their companions. Stellar masses were computed by Taylor et al. (2011) who used the *ugriz* photometry and local-flow-corrected spectroscopic redshifts (Tonry et al. 2000) to construct the rest-frame spectral energy distribution of each galaxy. These spectral energy distributions were used to model the stellar mass, star formation history, metallicity, and dust extinction in each galaxy assuming a Chabrier (2003) stellar initial mass function (IMF). These stellar mass estimates are accurate to approximately 0.1 dex for galaxies brighter than $r_{petro} = 19.8$ mag.

2.2.3 GAMA Galaxy Group Catalogue

The deep and spectroscopically complete nature of the GAMA survey has allowed the creation of one of the most robust catalogues of galaxy groups made to date. Robotham et al. (2011) used a friends-of-friends linking algorithm to assign galaxies to groups. This two-step process uses both the projected separations of the galaxies and their redshifts to recover the true grouping of galaxies in space. The nature of the algorithm used is such that even galaxies in pairs are assigned to groups. The grouping algorithm locates the central galaxy of a group and computes the group size, multiplicity (number of members above the detection limit), and velocity dispersion. From these measurements, it is possible to derive a number of properties of the group and its members including the total dynamical mass of the halo, the projected distance of each galaxy from the centre of the group, and the line-of-sight velocity of each galaxy with respect to the group centre. For an in-depth discussion of the group-finding algorithm used to derive the catalogue, see Robotham et al. (2011), though note that at the time the original paper was published, the GAMA survey was still ongoing and consequently the size of the group catalogue and the spectroscopic completeness have since increased.

2.3 Sample Selection

We have selected galaxies from the SAMI Galaxy Survey in the GAMA regions. This does not include galaxies that form part of the SAMI targeted cluster sample. At the time of writing there were 1295 galaxies from the SAMI main survey that have been observed and for which the data had been reduced. This study of the spatially resolved star formation properties of galaxies requires the selection of a set of star-forming galaxies. Our method for selecting our star-forming sample mimics that of Schaefer et al. (2017). To measure whether a galaxy has any ongoing star formation, we have integrated the data cubes across both spatial axes and from the resulting spectrum we measure the equivalent

[2] Astrophysics Source Code Library, ascl:1407.006 ascl.net/1407.006

width (EW) of the Hα emission, correcting for the underlying stellar absorption. If the absolute value of this EW is less than 1 Å we say that the galaxy is not star-forming. This corresponds to a specific star formation rate limit of approximately 10^{-12} yr^{-1}, and eliminates 253 galaxies from our sample. In addition to this constraint we classify galaxies based on their emission line ratios in the central 2″. Based on the ratios of [N II] λ6583 to Hα and [O III] λ5007 to Hβ in this inner spectrum, we classify galaxies as either star-forming, composite or AGN/LINER based on their location on the Baldwin, Phillips, & Terlevich (1981) diagram. Galaxies with line ratios that place them above both the Kewley et al. (2001) and Kauffmann et al. (2003c) lines are classified as AGN/LINER, of which we find 333 in our sample. Between these two constraints are a total of 165 composite objects and below both lines are the star-forming objects. To reduce the effect of having hexabundles with a finite aperture on measuring the spatial distribution of star formation we also limit the sizes of our galaxies that we include in our analysis. Twenty six galaxies with effective radii greater than 15″ are rejected, as are 149 galaxies for which the seeing of the observation is greater than r_e. We also excluded galaxies that have ellipticity values greater than 0.7 to eliminate 200 edge-on systems. Note that some galaxies have been rejected based on more than one constraint. Our final star-forming sample comprises 325 galaxies, including 158 galaxies not assigned to groups and 167 galaxies in groups.

2.4 Analysis of SAMI data

The analysis of the SAMI data is as described in Schaefer et al. (2017), but for completeness we shall summarise the process here.

2.4.1 Annular Voronoi Binning

To facilitate a robust correction for dust attenuation along the line of sight, we applied annular Voronoi binning to the SAMI data cubes. Spaxels are added together in elliptical annuli to a signal-to-noise ratio of 10 per Å in the continuum at the wavelength of the Hβ line. An adaptive binning scheme has the advantage of providing sufficient signal to allow the subtraction of the Hβ absorption line and thus an accurate correction for dust extinction. This binning additionally ensures that the spatial scale over which a single dust correction is applied is minimised, while further ensuring that the radial structure in each galaxy is preserved. We have binned the SAMI data in 0.″5-wide elliptical annuli that are defined by the ellipticity and position angle obtained from the GAMA Sèrsic photometry.

2.4.2 Spectral fitting with LZIFU

We fitted the spectrum within each annular Voronoi bin using LZIFU (Ho et al. 2016). LZIFU is a spectral fitting pipeline written in the Interactive Data Language (IDL). It utilises the Penalised Pixel Fitting algorithm (pPXF; Cappellari & Emsellem 2004) to model the stellar continuum light from each galaxy. For each spectrum we fitted a linear combination of simple stellar population (SSP) models from the MILES library (Vazdekis et al. 2010) with an 8th degree multiplicative polynomial to take into account any residual flux calibration errors and the reddening of the continuum from astrophysical sources. We used a 65 template subset of the full MILES library. This subset covers five metallicities from [Z/H] = −1.71 to 0.22 and thirteen ages spaced logarithmically in the range 0.063 − 14 Gyr. The continuum model derived by pPXF was subtracted from the data, and the emission lines, including Hα and Hβ, were fitted with single component Gaussians using the MPFIT routine (Markwardt 2009).

2.5 Star-forming properties of galaxies

We use a number of metrics to determine the impact of the group environment on the star formation in the galaxies in our sample.

2.5.1 Integrated star formation rates

We calculated the total star formation rate within the SAMI aperture by adding the dust-corrected flux from each annular Voronoi bin. Dust extinction corrections are applied by measuring the departure of the Balmer decrement, the ratio of measured Hα flux to Hβ flux (BD; $f_{\mathrm{H}\alpha}/f_{\mathrm{H}\beta}$), from the canonical value of 2.86 predicted for Case B recombination under standard conditions. Under the assumption that the intervening dust forms a foreground screen to the HII regions in our target galaxies (Calzetti 2001) and using the Cardelli, Clayton, & Mathis (1989) dust extinction curve, the obscuration-corrected Hα flux is

$$F_{\mathrm{H}\alpha} = f_{\mathrm{H}\alpha}\left(\frac{BD}{2.86}\right)^{2.36} \quad (1)$$

in each spectrum. In cases where the signal-to-noise ratio for the Hβ emission line is less than 3, or the measured Balmer decrement is less than 2.86, we assume no dust extinction and use the raw Hα flux. Integrating these dust-corrected fluxes over the SAMI aperture gives the integrated flux, which is converted to a luminosity using the redshift of each galaxy

$$L(\mathrm{H}\alpha) = \frac{F_{\mathrm{H}\alpha}}{4\pi d_L^2}, \quad (2)$$

where d_L is the luminosity distance to the galaxy. We calculate the star formation rates in our galaxies with the Kennicutt (1998) relation assuming a Chabrier (2003) IMF:

$$\mathrm{SFR} = \frac{L_{\mathrm{H}\alpha}\ (W)}{2.16\times10^{34}}\ \mathrm{M}_\odot\ \mathrm{yr}^{-1}. \quad (3)$$

2.5.2 The spatial distribution of star formation

We quantify the radial extent of star formation in galaxies within our sample by making use of the ratio $r_{50,\mathrm{H}\alpha}/r_{50,cont}$, described at length in Schaefer et al. (2017). This measurement compares the radius within which half of the dust-corrected Hα emission emanates to the radius containing half of the continuum light from the part of the galaxy that lies within the view of the SAMI hexabundles. These radii are calculated by measuring the curve-of-growth for

the emission or continuum light. In calculating the curves-of-growth we have made the assumption that galaxies in our sample are idealised thin discs and any ellipticity is due to their inclination to our line of sight. The ellipticity and position angle on the sky are taken from the GAMA Sèrsic photometric fits to SDSS r-band images. An in-depth discussion of the measurement, advantages of, and systematic effects that can arise by making this measurement on galaxies observed with 15″ integral field units can be found in Schaefer et al. (2017).

3 RESULTS

3.1 Group mass and star formation rates

There is a significant body of work in the literature that focusses on how the star formation rates of galaxies change with stellar mass and environment density (e.g. Peng et al. 2010, 2012; Alpaslan et al. 2015; Davies et al. 2016a). These results are generally based on large-scale spectroscopic or photometric surveys. With a sample size of 325 star-forming galaxies, our primary aim is not to duplicate the results of these large surveys. Instead we measure integrated star formation rates with the intention of using these values as a diagnostic for the enhancement or suppression of star formation in galaxies. We shall restrict ourselves to a comparison of the values of star formation rates internally within SAMI galaxies, and not compare to the rates derived by other surveys. This is due to the different treatment of aperture effects by us and by other surveys. See Richards et al. (2016) for a thorough discussion of this topic.

We quantify the effect of group environments on the star-forming properties of galaxies by comparing the specific star formation rates of galaxies in our sample to their stellar masses and the masses of their parent group haloes. In Figure 1 we split our entire sample into three intervals of halo mass. A non-grouped sample, which comprises galaxies that do not appear in the GAMA Galaxy Group Catalogue (Robotham et al. 2011), a low-mass group sample with groups that have multiple galaxies within halos of mass below $10^{12.5}\,\mathrm{M}_\odot$, and a high-mass group sample with galaxies in group halos more massive than $10^{12.5}\,\mathrm{M}_\odot$. This boundary was chosen to approximately evenly split the grouped galaxy sample in two. We note that group masses here are derived from the dynamics of galaxies within each halo. For galaxies in the ungrouped subsample, the method of Robotham et al. (2011) was unable to estimate the halo mass. Based on the tight correlation between total stellar mass within a group and its halo mass presented by Yang et al. (2007), we can estimate that the most massive halos in the ungrouped sample will be of order $10^{11} - 10^{12}\,\mathrm{M}_\odot$. We will not use this kind of estimate for the remainder of this paper. In the upper row of panels Figure 1, we show the specific star formation rates of star-forming galaxies using blue circles, and of passive galaxies with red triangles. Black points are the median values of the specific star formation rates for star-forming galaxies in bins of stellar mass. In all environments there is a sharp increase in the passive fraction of galaxies at approximately $10^{10.5}\,\mathrm{M}_\odot$ in agreement with numerous previous studies (e.g. Kauffmann et al. 2003b; Geha et al. 2012). In the two lowest density environments the fraction of passive galaxies below this stellar mass threshold is $5 \pm 2\%$ for ungrouped galaxies and $3 \pm 2\%$ for the groups below masses of $10^{12.5}\,\mathrm{M}_\odot$. In the highest halo mass bin, the fraction of passive galaxies below the $10^{10.5}\,\mathrm{M}_\odot$ stellar mass threshold in somewhat higher, estimated to be $23 \pm 4\%$, with these figures representing the fraction of passive galaxies over the entire mass range less than $10^{10.5}\mathrm{M}_\odot$.

In addition to the increasing passive fraction of galaxies in the most massive groups, the specific star formation rates of star forming galaxies are reduced in dense environments. The mean specific star formation rates of galaxies is reduced from $\log_{10}(\mathrm{sSFR/yr}^{-1}) = -10.19 \pm 0.03$ in ungrouped galaxies, to $\log_{10}(\mathrm{sSFR/yr}^{-1}) = -10.35 \pm 0.05$ in the high-mass group sample. The reduction in the star formation rates of galaxies in massive groups relative to the non-grouped sample is manifest in the changing of the distribution of sSFRs between the two environments. This is demonstrated in Figure 2, which shows that the peak of the distribution in massive halos moves towards lower sSFRs with an asymmetry in the distribution imposed by a substantial tail towards lower values, and fewer galaxies with star formation rates above the non-grouped main sequence. The two-tailed Kolmogorov-Smirnov statistic for these two distributions is $D = 0.18$ with $p = 0.03$, which implies a difference between the two distributions at the 2σ significance level.

While star formation appears to be suppressed in some galaxies in groups with masses above approximately $10^{12.5}\,\mathrm{M}_\odot$, Figure 1 shows the enhancement of star formation in galaxies in groups below this halo mass threshold. In the top row of panels we show the specific star formation rates of galaxies observed by SAMI as a function of their stellar mass in three bins of group halo mass. The top row shows that the slope of the star formation rate main sequence is steeper for galaxies in low mass groups compared to ungrouped systems by 0.16 ± 0.09. This change in slope represents an enhancement of star formation in higher mass galaxies in these low mass groups. Galaxy groups in this mass range typically have less than four members, with ~ 40 per cent of galaxies in this sample residing in groups with only two members at the depth of the GAMA survey spectroscopy. Galaxies at the higher mass end of this scale represent the most massive systems in these groups, and thus our observations agree with the enhancement of star formation reported by Davies et al. (2015).

3.2 The spatial extent of star formation in galaxy groups

We can estimate the spatial extent of ongoing star formation using the scale-radius ratio, $r_{50,\mathrm{H}\alpha}/r_{50,cont}$ for each galaxy in our star-forming sample. When this ratio is large, the star formation is spatially extended and occurs in the disc of the galaxy. When the ratio is small, the majority of star formation is occurring in the central parts of the galaxy. We compare this ratio to the galaxy stellar mass in the same three bins of group mass in Figure 3. The data show that galaxies in the most massive groups have more centrally concentrated star formation on average. Within each bin of group halo mass, the relationship between the stellar mass and the spatial extent of star formation changes. For ungrouped galaxies there is no correlation between the stellar mass and $r_{50,\mathrm{H}\alpha}/r_{50,cont}$. This is consistent with the

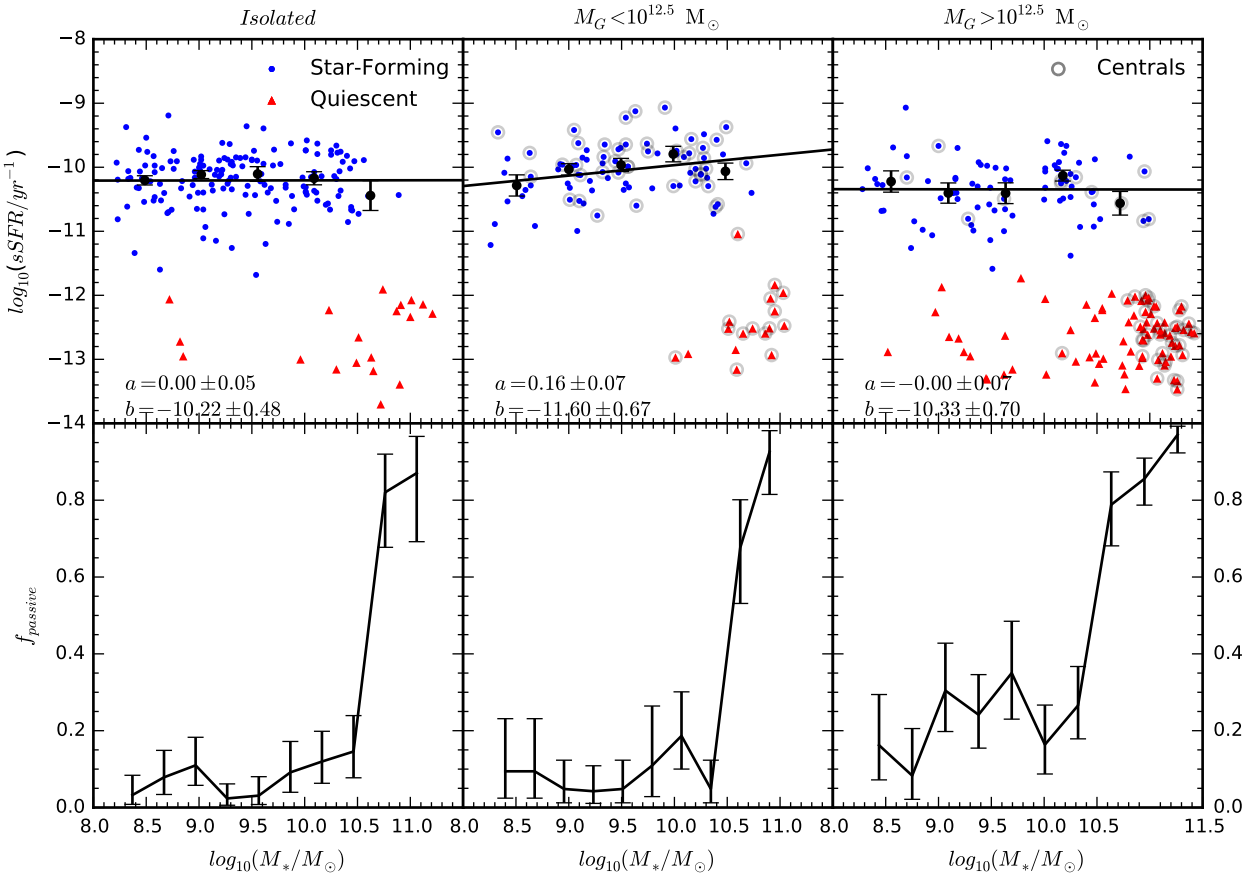

Figure 1. The top row shows the specific star formation rates of star-forming (blue points) and passive (red triangles) galaxies as a function of $\log_{10}(M_*/M_\odot)$ in different group environments. We have fitted a straight line of the form $\log_{10}(\mathrm{sSFR/yr}) = a \times \log_{10}(\mathrm{M_*/M_\odot}) + b$ to the star-forming galaxies in each bin of group environment and drawn this fit in solid black on the corresponding panel. The parameters for this fit are displayed at the bottom left of each panel. The lower row shows the fraction of galaxies that were classified as passive in bins of stellar mass. For ungrouped galaxies and galaxies in low-mass groups, the passive fraction in galaxies with stellar masses below $10^{10.5}\,\mathrm{M}_\odot$ is $5 \pm 2\%$. In the higher mass groups the passive fraction of galaxies rises to $23 \pm 4\%$ for galaxies below the $\mathrm{M_*} = 10^{10.5}\,\mathrm{M}_\odot$ threshold.

Table 1. The scale-radius ratio of galaxies split into bins of stellar mass and group halo mass. $\langle \log_{10}(r_{50,H\alpha}/r_{50,cont}) \rangle$ is the average log scale-radius ratio, σ is the standard deviation of the log scale-radius ratio and f_{cen} is the fraction of galaxies with $\log_{10}(r_{50,H\alpha}/r_{50,cont}) < -0.2$.

		Ungrouped	$\log_{10}\left(\frac{M_G}{M_\odot}\right) < 12.5$	$\log_{10}\left(\frac{M_G}{M_\odot}\right) \geqslant 12.5$
$\log_{10}\left(\frac{M_*}{M_\odot}\right) < 10$	$\langle \log_{10}(r_{50,H\alpha}/r_{50,cont}) \rangle$	-0.013 ± 0.009	-0.025 ± 0.012	-0.041 ± 0.018
	σ	0.093 ± 0.010	0.086 ± 0.009	0.126 ± 0.017
	f_{cen}	$0.04^{+0.02}_{-0.02}$	$0.05^{+0.03}_{-0.02}$	$0.10^{+0.05}_{-0.04}$
$\log_{10}\left(\frac{M_*}{M_\odot}\right) \geqslant 10$	$\langle \log_{10}(r_{50,H\alpha}/r_{50,cont}) \rangle$	-0.005 ± 0.010	-0.063 ± 0.017	-0.124 ± 0.020
	σ	0.064 ± 0.010	0.089 ± 0.012	0.122 ± 0.011
	f_{cen}	$0.04^{+0.04}_{-0.03}$	$0.06^{+0.06}_{-0.04}$	$0.29^{+0.08}_{-0.07}$

findings of Schaefer et al. (2017), where we found no dependency of the scale-radius ratio on the stellar mass of galaxies in a smaller sample. Within groups, however, this is not the case. Galaxies in groups with $M_G < 10^{12.5}\,\mathrm{M}_\odot$ show a slight tendency to display smaller scale-radius ratios, particularly with increasing stellar mass. In these environments, the Spearman rank correlation coefficient between $\log_{10}(\mathrm{M_*/M_\odot})$ and $r_{50,\mathrm{H}\alpha}/r_{50,cont}$ is $\rho = -0.30$ with $p = 0.005$. In groups with $M_G > 10^{12.5}\,\mathrm{M}_\odot$ the strength of this correlation is increased to $\rho = -0.40$, $p = 0.0002$. In galaxy groups with halo masses above $10^{12.5}\,\mathrm{M}_\odot$, galaxies with stellar masses above $\sim 10^{10}\,\mathrm{M}_\odot$ will display star formation on a shorter radial scale than for similar ungrouped galaxies. For galaxies with stellar masses less than $\sim 10^{10}\,\mathrm{M}_\odot$, the spatial extent of star formation appears to be independent of the halo mass that the galaxy occupies.

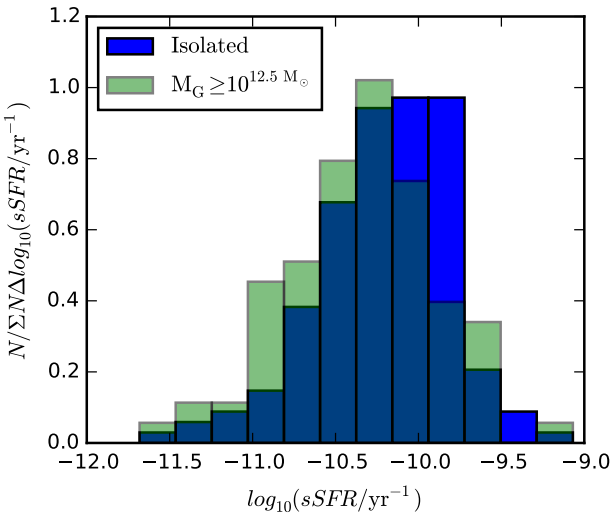

Figure 2. The normalised distribution of specific star formation rates for non-grouped galaxies (blue) and galaxies in groups with $M_G > 10^{12.5}\,M_\odot$ (green).

These results are summarised in Table 1, wherein we define galaxies as having 'centrally concentrated' star formation if $\log_{10}(r_{50,H\alpha}/r_{50,cont}) < -0.2$ following Schaefer et al. (2017). This threshold was chosen to be 2 standard deviations below the mean for ungrouped galaxies. For galaxies with stellar masses greater than $10^{10}\,M_\odot$, the fraction of galaxies that display this centrally-concentrated star formation rises from $4^{+4}_{-3}\%$ in ungrouped galaxies, to $29^{+8}_{-7}\%$ in groups more massive than $10^{12.5} M_\odot$. For galaxies below this stellar mass threshold, there is no statistically significant change in the fraction of centrally concentrated star formers with group mass. In both ranges of galaxy stellar mass, the standard deviation from the mean of $r_{50,H\alpha}/r_{50,cont}$ increases in groups with halo mass greater than $10^{12.5}\,M_\odot$. In low and high stellar mass samples, the standard deviation in the scale-radius ratio increases by 0.033 ± 0.020 and 0.058 ± 0.015 respectively.

While Figure 3 shows that increased group mass tends to change the distribution of star formation in galaxies, it does not directly inform us whether it is associated with the quenching of star formation. In Figure 4 we examine the relationship between the specific star formation rates of galaxies with the spatial extent of star formation as described by $r_{50,H\alpha}/r_{50,cont}$ in different group environments. To highlight the qualitative differences in the quenching mechanisms at different stellar masses, we have divided our sample into three intervals of stellar mass. The various correlations for each stellar mass and environment interval are highlighted in Table 2.

For galaxies with $M_* > 10^{10.1}\,M_\odot$ that are either ungrouped or in group halos less massive than $10^{12.5}\,M_\odot$ there is a significant anti-correlation between the specific star formation rate and $r_{50,H\alpha}/r_{50,cont}$, with Spearman's $\rho = -0.36$ and $p = 0.007$. In these environments an increase in the specific star formation rates of galaxies is associated with star formation occurring more readily in the centres of the galaxies. The reduction of star formation occurs with star formation persisting on a relatively extended radial scale. For galaxies with $M_* > 10^{10.1}\,M_\odot$ in haloes more massive than $10^{12.5}\,M_\odot$ the distribution of star formation behaves differently as star formation is reduced. For the massive group sample the specific star formation rate correlates positively with $r_{50,H\alpha}/r_{50,cont}$. As star formation is reduced in these galaxies, it becomes more confined towards the centres of galaxies, indicating that the onset of environmental quenching occurs in the outskirts of these galaxies. The outside-in quenching of star formation is the dominant form of environmental quenching in galaxies more massive than $10^{10}\,M_\odot$ in group haloes more massive than $10^{12.5}\,M_\odot$, while less massive galaxies have their star formation shut down more uniformly across their discs.

3.2.1 *Central enhancement of star formation in massive groups?*

We have calculated the central star formation rate surface density in a central 1″ aperture in each of the star-forming galaxies in our sample. We have used these values to test whether the central enhancement of star formation is able to explain the reduction in scale-radius ratio in high-mass groups. For galaxies with stellar masses in the range $10^{10} < M_*/M_\odot < 10^{10.5}$, compare the average central star formation rate surface density for normal galaxies and those with centrally concentrated star formation. This limited range of stellar mass was chosen to minimise the We find that in groups with halo mass greater than $10^{12.5}\,M_\odot$ the mean central star formation rate surface density is $\log_{10}(\Sigma_{sfr}/M_\odot\,yr^{-1}\,kpc^{-1}) = -1.41 \pm 0.11$ and $\log_{10}(\Sigma_{sfr}/M_\odot\,yr^{-1}\,kpc^{-1}) = -1.9 \pm 0.19$ for normal and centrally-concentrated star-formers respectively. This yields a difference of 0.21 ± 0.31, which is below one sigma significance. The central star formation rate surface density in galaxies with centrally concentrated star formation is not significantly different from other galaxies with similar stellar mass in the same environments.

3.2.2 *The spatial extent of star formation and the colour-mass diagram*

The position of a galaxy on the colour mass diagram is commonly used diagnose its current evolutionary state. Galaxies in the blue cloud are often star forming or have had a recent burst of star formation, while galaxies in the red sequence are often passive and have no evidence of star-formation within the last several giga years. Galaxies in between the blue cloud and red sequence are often considered to be in the process of being quenched or having their star formation rejuvenated. We display the locations of the galaxies from our star-forming sample in this parameter space in Figure 5, dividing the sample into bins of group mass. In general galaxies with $u - r$ colours placing them between the blue cloud and red sequence tend to have more centrally concentrated Hα emission. This is especially visible in groups with mass greater than $10^{12.5}\,M_\odot$. As galaxies in groups more massive than $10^{12.5}\,M_\odot$move away from the blue cloud, their star formation becomes more centrally concentrated.

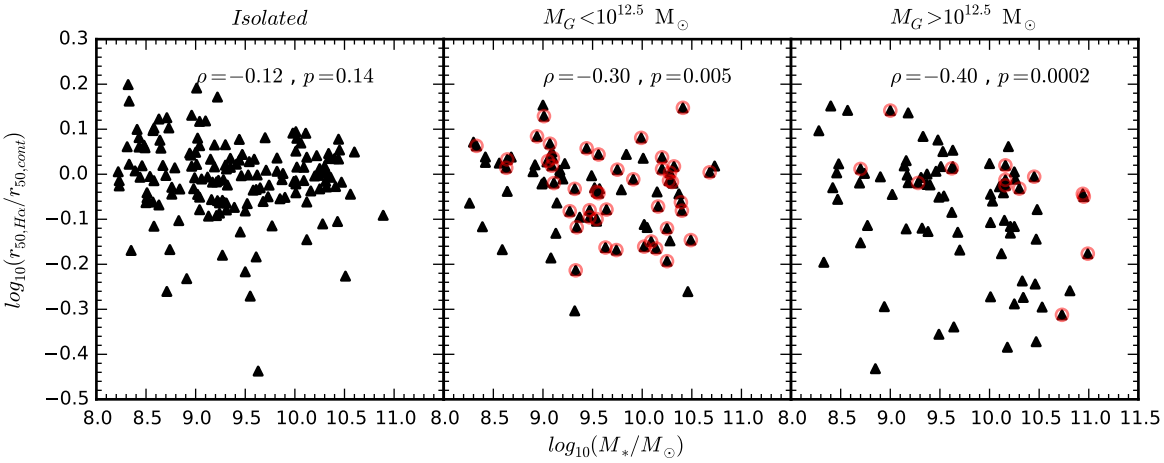

Figure 3. The scale-radius ratio as a function of stellar mass in different intervals of galaxy group halo mass. In the upper right of each panel we show the Spearman rank correlation coefficient and the associated p-value. For the ungrouped sample there is no statistically significant correlation, but in progressively more massive groups, more massive galaxies appear to have more centrally concentrated star formation on average. Galaxies that have been identified as the centrals in their halos are make with a red circle.

Table 2. Correlation coefficients for data displayed in Figure 4. ρ is the Spearman rank correlation coefficient between the specific star formation rate and the scale-radius ratio in bins of stellar mass indicated in the first column, and in bins of group halo mass indicated in the top row.

	Ungrouped, $M_G < 10^{12.5}$	$M_G > 10^{12.5}$	$P(\rho_1 = \rho_2)$
$8.2 < \log_{10}(M_*/M_\odot) < 9.1$	$\rho = 0.09$, $p = 0.42$	$\rho = 0.32$, $p = 0.18$	0.9σ, $p = 0.19$
$9.1 < \log_{10}(M_*/M_\odot) < 10.1$	$\rho = -0.20$, $p = 0.04$	$\rho = -0.17$, $p = 0.36$	0.17σ, $p = 0.63$
$10.1 < \log_{10}(M_*/M_\odot) < 11.0$	$\rho = -0.36$, $p = 0.007$	$\rho = 0.46$, $p = 0.009$	3.7σ, $p = 0.0001$

3.3 Satellites and centrals

Galaxies that are environmentally quenched may experience different processes that shut down their star formation depending on where they sit within their parent group halo. A galaxy that is at the centre of a group will be less likely to experience, for example, ram pressure stripping, than a galaxy that is its satellite. In galaxy groups that are dynamically relaxed, the most massive object will tend to sit at the centre of the halo, but this is not always the case. The group catalogue of Robotham et al. (2011) calculates an iterative group centre that is robust to the effects of massive galaxies in falling into groups. In this process the galaxy that is most distant from the centre of light of the group is rejected and the centre of light is recalculated. This process is repeated until two galaxies remain, at which point the brightest of that pair is decided as the iterative centre. Robotham et al. (2011) reports that in 95 per cent of cases the iterative centre is the same as the brightest group galaxy. We term galaxies in our sample that are identified as the iterative centre of their group as 'centrals' and all other group galaxies as 'satellites'.

In groups less massive than $10^{12.5}\,\mathrm{M}_\odot$, the number of centrals in our sample is higher, representing a total of 48 of the 92 star-forming galaxies in this group mass bin. These galaxies preferentially occupy the higher end of the mass distribution and seem to drive the apparent enhancement of star formation seen in the low-mass group sample in the central panel of Figure 1.

Galaxies that are the centrals of massive groups are by definition rare, and having high stellar mass are often passive. Of the 92 star-forming galaxies in groups more massive than $10^{12.5}\,\mathrm{M}_\odot$, only 12 are centrals. This low number means that we are unable to make definitive statements about whether the spatial distribution of star formation in centrals differs in comparison to the star formation distribution in satellite galaxies in massive groups. In the right-hand panel of Figure 3 we see that the average scale-radius ratio for central galaxies is higher than for satellites. The reported correlation coefficient between $\log_{10}(M_*)$ and $\log_{10}(r_{50,\mathrm{H}\alpha}/r_{50,cont})$ goes from $\rho = 0.40$, $p = 0.0002$, to $\rho = 0.41$, $p = 0.0005$, but we note that at all stellar masses, the star formation radial scale is higher for central galaxies in our sample than for satellite galaxies.

In Figure 4, we showed that the scale-radius ratio in galaxies with stellar masses greater than $10^{10.1}\,\mathrm{M}_\odot$ in groups with halo mass greater than $10^{12.5}\,\mathrm{M}_\odot$ correlated with their specific star formation rates. Galaxies that are environmentally quenched in these massive groups tend to have their star formation suppressed in their outskirts first. This trend was indicated by black crosses in the lower panel of Figure 4, and included both satellites and centrals. If we remove the central galaxies from this subsample we increase the strength of the correlation and its significance to $\rho = 0.53$ with $p = 0.006$, though the sample size is reduced to just 26 galaxies.

3.4 Galaxy-galaxy tidal interactions

A number of authors have suggested that dynamical disturbances driven by tidal interactions between galaxies in

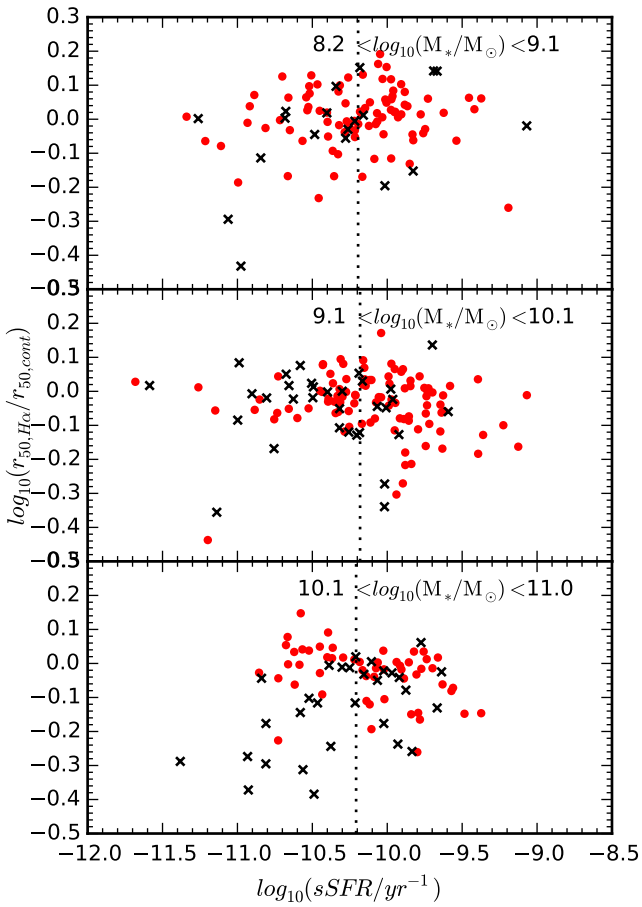

Figure 4. The scale-radius ratio as a function of the specific star formation rates of galaxies in the stellar mass intervals shown at the top of each panel. Red points represent galaxies that are either not in groups or are in groups with halo mass less than $10^{12.5}\,\mathrm{M}_\odot$, while black crosses are galaxies in haloes more massive than $10^{12.5}\,\mathrm{M}_\odot$. The distribution of star formation in galaxies as they move below the star formation rate main sequence depends on their stellar mass. In the two lowest stellar mass intervals, the star formation remains relatively extended across all environments. In the highest mass galaxies this is not the case. For the low halo mass sample there is a significant anti-correlation between specific star formation rate and the spatial extent of star formation, with Spearman $\rho = -0.36$, $p = 0.007$. For the high-mass group sample, the correlation is reversed, with Spearman's $\rho = 0.46$, $p = 0.009$. The vertical black dotted lines represent the mean specific star formation rate for ungrouped galaxies in each mass bin.

groups can cause gas to fall towards the centres of galaxies (e.g. Hernquist 1989; Moreno et al. 2015). While this may cause the enhancement of star formation on short timescales, the consumption of gas by star formation induced by the interaction will ultimately cause the galaxy to become quenched earlier than in ungrouped galaxies. We can estimate the strength of the current tidal interaction using the perturbation parameter of Dahari (1984) and Byrd & Valtonen (1990),

$$P_{gc} = \left(\frac{M_c}{M_g}\right) \times \left(\frac{r_g}{d_{gc}}\right)^3, \quad (4)$$

where M_c is the mass of the companion, M_g is the mass of the galaxy being perturbed, r_g is the optical size of the galaxy and d_{gc} is the projected distance between the galaxy and its companion. Dahari (1984) and Byrd & Valtonen (1990) defined this r_g in terms of the optical sizes of galaxies as measured by hand from photographic plates, so we shall approximate this with the r-band r_{90}, the radius that contains 90% of the flux, as given by the GAMA Sérsic photometric fits. Byrd & Valtonen (1990) showed that gas infall is expected when the perturbation parameter is greater than $\sim 0.01 - 0.1$, depending on the halo-to-disc mass ratio. We have calculated the perturbation parameter for all possible pairs of galaxies in the GAMA Galaxy Group Catalogue, and use the greatest perturbation within a group to estimate the tidal effects on a galaxy. Using this estimator of the strength of the tidal forces experienced by each galaxy in the group we find no evidence that tidal interactions change the radial extent of star formation in galaxy groups. This is shown in Figure 6. We must note that this does not necessarily imply that tidal interactions have no effect on the distribution of star formation in galaxies because there could be a considerable time delay between a tidal interaction and the movement of gas to the centres of the galaxies.

3.5 Tidal interactions with the group potential

The galaxy groups in this sample can be as massive as $10^{14}\,\mathrm{M}_\odot$. This means that tidal perturbations in individual galaxies can be caused by their gravitational interaction with the group potential as a whole. For a galaxy with mass M_g with radius r_g located at a distance d from the centre of a group halo of mass M_G, the tidal perturbation is given by

$$P_{Gg} = \left(\frac{M_G}{M_g}\right) \times \left(\frac{r_g}{d}\right)^3, \quad (5)$$

following Boselli & Gavazzi (2006). We calculate these values using the group mass and group-centric distances provided by the GAMA Galaxy Group Catalogue, and compare it to the various properties of the galaxies. In Figure 7 we compare the group tidal perturbation to various measures of the star formation rate and distribution in our sample. We find no correlation between the group tidal perturbation and the star-forming properties of the galaxies. This does not necessarily imply that tidal interactions with the group potential do not alter the properties of galaxies as the metric for tidal perturbation used has large systematic uncertainties. Each galaxy's distance d from the centre of the group is subject to projection effects, in addition to the group centre being poorly defined for groups with only several members. The use of stellar masses for the mass of each galaxy is also systematically low; the amount of dark matter in each galaxy is unknown but likely higher than the stellar mass.

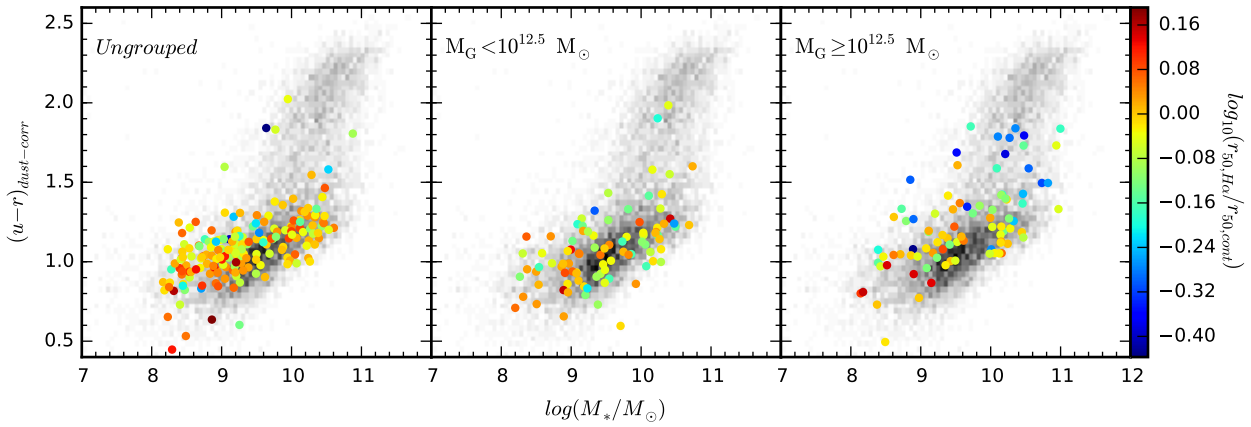

Figure 5. The position of galaxies in our star-forming sample on the $\log_{10}\mathrm{M}_*/\mathrm{M}_\odot$ vs dust-corrected, rest-frame $u-r$ colour plane. Each panel shows an interval of group halo mass, The greyscale background represents the stellar mass and intrinsic $u-r$ colour of galaxies in the GAMA survey with $z<0.1$, while the coloured points show the scale-radius ratio measured in SAMI galaxies. From left to right the panels include SAMI galaxies that are ungrouped, have measured group masses less than $10^{12.5}\,\mathrm{M}_\odot$ and have group masses above $10^{12.5}\,\mathrm{M}_\odot$. The colour scale is the same across all three group mass bins.

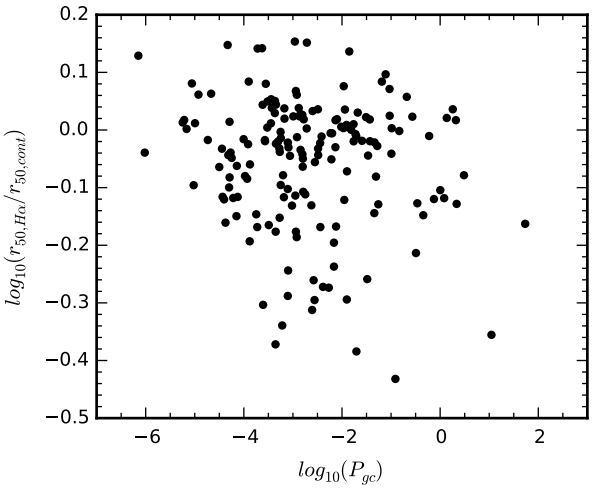

Figure 6. The scale-radius ratio as a function of the tidal perturbation parameter for galaxies in groups. With a Spearman rank correlation coefficient of $\rho=-0.06$ with $p=0.41$, there is no evidence that the current tidal perturbation influences the radial distribution of star formation in these galaxies.

3.6 Projected phase space

Some recent works have made use of projected phase space diagrams as a means of diagnosing particular processes that may be acting on galaxies in clusters (e.g. Oman et al. 2013; Jaffé et al. 2015; Oman & Hudson 2016). In this scheme galaxies are placed in phase space with position and velocity measured relative to the host halo. Galaxies with velocities greater than the group velocity dispersion and within $0.5\,r_{200}$ are likely to undergo ram pressure stripping, low velocity galaxies far from the group centre are likely to be on their first passage through the group, and slow-moving galaxies close to the group centre are likely virialised within the group.

We calculate r_{200} for the groups in our sample using the prescription of Finn et al. (2005),

$$r_{200}=1.73\frac{\sigma_v}{1000\,\mathrm{km\,s^{-1}}}\frac{1}{\sqrt{\Omega_0+\Omega_\Lambda(1+z)^3}}h_{100}^{-1}\,\mathrm{Mpc}, \quad (6)$$

where σ_v is the group velocity dispersion and z is the systemic redshift of the group.

In Figure 8 we display galaxies in groups more massive than $10^{12.5}\,\mathrm{M}_\odot$ in projected phase space. Galaxies showing centrally concentrated star formation ($\log_{10}(r_{50,H\alpha}/r_{50,cont})<-0.2$) seem to follow the same distribution in projected phase space as other star-forming galaxies. A two-sample Kolmogorov-Smirnov test comparing the centrally concentrated star formers to the normal star-forming galaxies along each dimension of projected phase-space showed that the distributions are not significantly different. In group-centric radius the K-S statistic is $D=0.21$ with p-value 0.62, and in relative velocity the K-S statistic is $D=0.24$ with p-value 0.46.

All but one of the galaxies that have been identified as having centrally concentrated star formation exist within r_{200} of their respective groups, and most have line-of-sight velocities relative to the group less than the group velocity dispersion. This may suggest that these systems are virialised and have existed in the groups for some time.

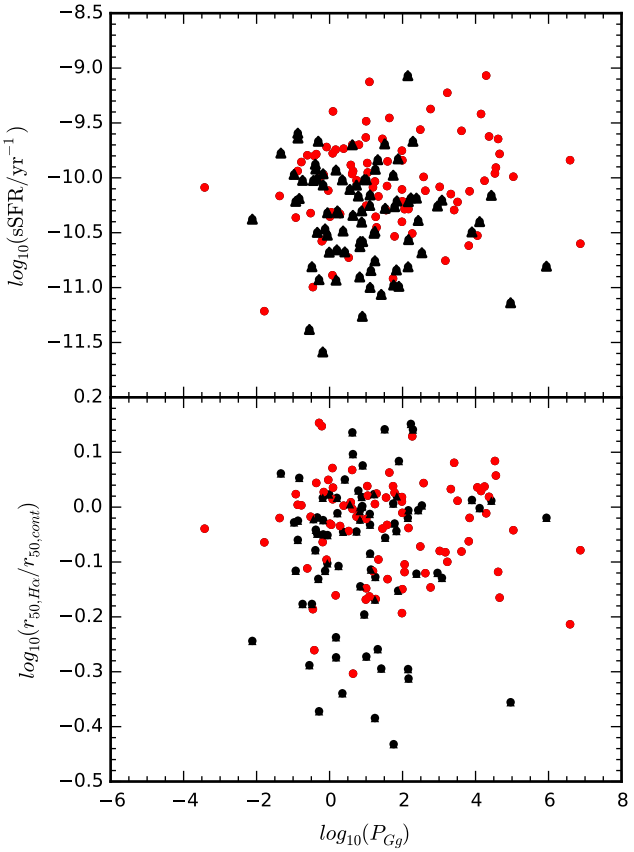

Figure 7. The star-forming properties of galaxies as a function of group tidal perturbation parameter. In the upper, middle and lower panels we compare respectively the specific star formation rate, scale radius ratio and central Hα equivalent width to the group tidal perturbation parameter, P_{Gg}. Black points denote galaxies in groups more massive than $10^{12.5}\,\mathrm{M}_\odot$ and red points indicate galaxies in lower mass groups.

3.7 Distribution of star formation vs group-centric radius

In Section 3.6 we saw that the distribution of centrally concentrated star-forming galaxies in groups more massive than $10^{12.5}\,\mathrm{M}_\odot$ is not significantly different for other star-forming systems in projected phase space. We find no strong trend between $r_{50,H\alpha}/r_{50,cont}$ and group-centric radius for galaxies within groups. To highlight the difference between the galaxy populations within and outside of galaxy groups, we have matched galaxies from the ungrouped sample to the nearest group halo, within $\pm 1000\,\mathrm{km\,s^{-1}}$ from the matched group systemic velocity. Figure 9 shows the scale-radius ratio in galaxies in and around groups more massive than $10^{12.5}\,\mathrm{M}_\odot$. Within these groups, closer than r_{200} to the centre of the group, there is no correlation between r_g and $r_{50,H\alpha}/r_{50,cont}$. For galaxies with $M_* > 10^{10}\,\mathrm{M}_\odot$ there is an apparent boundary at $r_g \sim r_{200}$, outside of which there are relatively few galaxies with the signatures of centrally confined star formation. Within r_{200}, the fraction of star-forming galaxies with centrally concentrated star formation rises from 7^{+7}_{-4} per cent to 35^{+9}_{-8} per cent[3]. The location of a galaxy within r_{200} of a group with halo mass greater than $10^{12.5}\,\mathrm{M}_\odot$ appears to be the primary factor in determining the outside-in quenching of star formation.

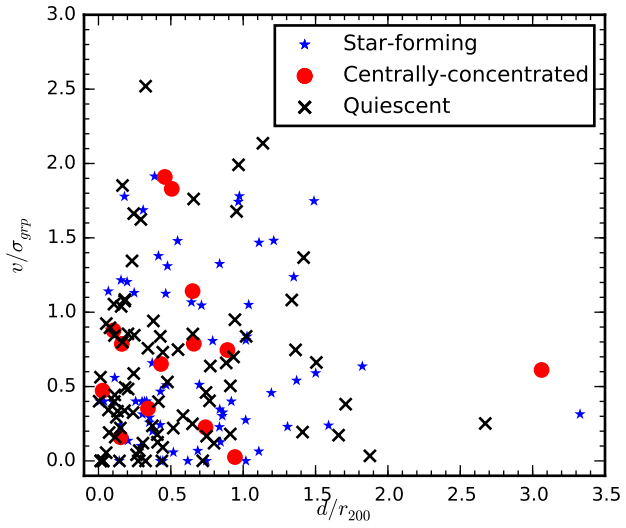

Figure 8. Projected phase space diagram for galaxies in groups with $M_H > 10^{12.5}\,\mathrm{M}_\odot$. The horizontal axis is the distance each galaxy is from the centre of the group, in units of r_{200}. The vertical axis is the velocity of each galaxy relative to the systemic velocity of the group compared to the velocity dispersion of the group. Blue stars and red circles are star-forming galaxies, and black crosses are passive galaxies. Red circles represent star-forming galaxies with centrally concentrated star formation.

3.8 Nearest neighbour interactions

Data from large-scale surveys has suggested that interactions between galaxies and their nearest neighbours may be able to either enhance or suppress star formation (e.g. Patton et al. 2013; Davies et al. 2015). To test this with SAMI, we use nearest-neighbour distances from the GAMA spectroscopic catalogue, including galaxies that are not necessarily in the group catalogue, but are more luminous than $\mathrm{M}_r = -18.5$. For the sample as a whole, we find no dependence of the specific star formation rates of galaxies on the distance to the nearest neighbour, though we note that our sample size is several orders of magnitude smaller than the large samples acquired through single-fibre spectroscopy. The ratio $r_{50,H\alpha}/r_{50,cont}$ appears to be reduced at small separations between galaxies, but the nearest-neighbour distance is strongly correlated with group mass, obscuring any strong conclusion. To resolve this issue we performed a partial Spearman rank correlation analysis between the group mass, nearest-neighbour distance, and $r_{50,H\alpha}/r_{50,cont}$ ratio for galaxies with group mass estimates. When the

[3] These fractions differ slightly, but not significantly from the fractions presented in subsection 3.2. This is because those fractions included galaxies that are associated with a group, but may have been further than r_{200} from the group centre.

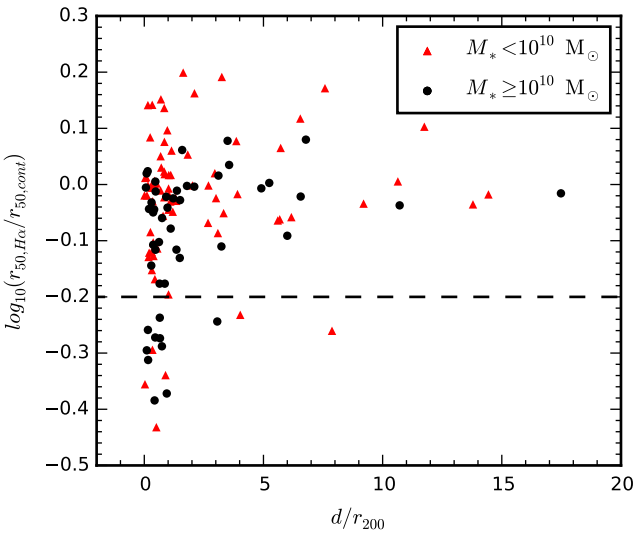

Figure 9. The scale radius ratio for galaxies as a function of distance from the centre of the nearest group. This sample includes both galaxies that are in the GAMA Galaxy Group Catalogue and galaxies whose nearest group halo is more massive than $10^{12.5}\,\mathrm{M}_\odot$. The horizontal dashed line is the fiducial $\log_{10}(r_{50,H\alpha}/r_{50,cont}) = -0.2$ dividing line below which we say a galaxy has centrally concentrated star formation. For $M_* > 10^{10}\,\mathrm{M}_\odot$, galaxies with centrally concentrated star formation exist almost exclusively within r_{200}, though there is no correlation with projected group-centric distance within r_{200} in these groups. For galaxies less massive there is no radial trend at all, and the fraction of galaxies with $\log_{10}(r_{50,H\alpha}/r_{50,cont}) = -0.2$ is consistent with the scatter in the distribution.

group mass is taken into account, the spearman rank correlation coefficient between nearest neighbour distance and $r_{50,H\alpha}/r_{50,cont}$ is found to be small and not significant ($\rho = 0.09\,, p = 0.26$).

4 DISCUSSION

Taking advantage of the SAMI Galaxy Survey and the GAMA Galaxy Group Catalogue we have presented the relationships between the spatial extent of star formation and the total star formation rate with a number of metrics for local environment. The rationale behind this is that the signatures of particular quenching mechanisms will be most sensitive to the environment measures that best represent those processes. Based on the conclusions of previous authors we have identified tidal interactions, strangulation and ram pressure stripping as the primary candidates for quenching star formation in galaxy groups.

Our analysis has focussed on two measurements of the star formation that tell us about the nature of any quenching that is taking place. We study the specific star formation rate that tells us whether each type of environment is enhancing or suppressing star formation globally within a galaxy. In addition to the specific star formation rate we include the scale-radius ratio, which provides information on the radial extent of star formation.

The SAMI data show that the mass of the group halo that a galaxy occupies is a good predictor of the signatures of star formation quenching. Broadly, we find two intervals of group halo mass within which the star forming properties of galaxies differ from each other and from an ungrouped sample. These are discussed below.

4.1 Massive groups, $\mathrm{M}_G > 10^{12.5}\,\mathrm{M}_\odot$

Galaxies in more massive groups are more likely to be quenched, and star-forming galaxies in more massive groups have lower specific star formation rates. Moreover, galaxies in groups with $\mathrm{M_G} > 10^{12.5}\,\mathrm{M}_\odot$ with stellar masses greater than $\sim 10^{10}\,\mathrm{M}_\odot$ will have more centrally concentrated star formation, while galaxies with stellar masses less than $10^{10}\,\mathrm{M}_\odot$ have more spatially extended star formation. In both brackets of stellar mass, the specific star formation rate is anti-correlated with halo mass. This trend, highlighted in Figure 3, indicates a qualitative difference in the way that star formation quenching proceeds for galaxies at different stellar masses. While this observation alone does not tell us what the mechanism is, it does have two implications for our understanding of the quenching process:

(i) The environmental quenching of star formation is not an instantaneous process in group galaxies over the stellar mass range $8 < \log_{10}(\mathrm{M}_*/\mathrm{M}_\odot) < 11$ in halos up to $\mathrm{M}_G = 10^{14.5}\,\mathrm{M}_\odot$. If this were not the case, we would not see the lowering of the average specific star formation rate by 0.15 ± 0.06 dex in the most massive groups.

(ii) Either *a*) low-mass galaxies quench by a mechanism that is different than for high-mass galaxies, or *b*) a single mechanism causes the effects that we observe, but this mechanism affects the distribution of star formation in a way that depends on the stellar mass.

In table 1 we quantified the increased scatter of $r_{50,\mathrm{H}\alpha}/r_{50,cont}$ in the high mass group sample. This increase in scatter is preferentially downward, that is, while some galaxies in more massive groups have star formation radial distributions that are similar to those in ungrouped galaxies, a significant fraction have more centrally concentrated star formation, and very few have more extended star formation. In particular, 29^{+8}_{-7} per cent of galaxies more massive than $M_* = 10^{10}\,\mathrm{M}_\odot$ in the massive group sample have centrally-concentrated star formation, compared to 4^{+2}_{-2} per cent in ungrouped galaxies. The increase in the scatter in $r_{50,\mathrm{H}\alpha}/r_{50,cont}$ shows the inefficiency of the outside-in quenching process. It is not clear whether this process acts on all galaxies that fall into these groups, or whether the inclination of the galaxy disc to the direction of passage through the intergalactic medium influences the change in the star formation distribution, as has been predicted by simulations of ram pressure stripping in galaxy groups and clusters (e.g. Bekki 2014).

We find that for galaxies that are identified as being the central object within their halo, at a given stellar mass the scale-radius ratio is higher than for satellite galaxies. For galaxies more massive than $10^{10.1}\,\mathrm{M}_\odot$, considering only the satellite galaxies increases the strength of the correlations between stellar mass and scale-radius ratio and specific star formation rate and scale-radius ratio. The difference between the spatial distribution of star formation in satellites

and centrals in massive groups is consistent with what previous authors (e.g. Peng et al. 2012) have concluded about the nature of environmental quenching. These authors have suggested that ram pressure stripping is a viable mechanism for the quenching of star formation in satellite galaxies.

4.2 Low-mass groups, $M_G < 10^{12.5}\,M_\odot$

In contrast to the environmental suppression of star formation in galaxies in the high-mass group sample, we find that for galaxies in low-mass groups (that is, with halo mass $M_G < 10^{12.5}\,M_\odot$), there is little evidence for environmental quenching in galaxies with stellar masses over $10^{10}\,M_\odot$. We find that in these systems star formation is enhanced. Galaxies with stellar masses above $\sim 10^{10}\,M_\odot$ appear to have their mean specific star formation rates boosted by 0.2 ± 0.09 dex above the mean for ungrouped galaxies in the same stellar mass range. This enhancement was driven by the central galaxies in these low-mass groups. A similar effect was noted by Davies et al. (2015) when studying the star formation rates of pairs of galaxies in the GAMA catalogue. They showed that the more massive galaxies in pairs have centrally enhanced star formation, while the lower mass companion had its star formation suppressed.

A similar trend is reflected in our data and we are able to study how this enhancement is produced in our galaxies. It is unclear whether we are observing the same trend as Davies et al. (2015), who observed enhancement of the star formation in only late-stage mergers, and we have a substantially smaller sample and less coverage of small separation pair galaxies.

In Figure 4 we investigated the radial extent of the star formation in galaxies as a function of their specific star formation rate. Ungrouped galaxies and those situated in low-mass group environments tend to have more centrally concentrated star formation as their specific star formation rates increase, while those with the lowest specific star formation rates tend to have extended Hα morphologies. This picture is broadly consistent with the simulations presented by Moreno et al. (2015), who showed that a close encounter between two galaxies will trigger the enhancement of star formation in a galaxy's centre.

4.3 Other metrics for interaction

4.3.1 Tidal Interactions

We do not find any significant correlation between the estimated strength of the tidal interaction between galaxies and their star-forming properties. The apparent strength of the tidal force acting on a galaxy, calculated from Equation 4, influences neither the total measured specific star formation or the scale radius of star formation relative to the scale radius of the stellar light. Superficially this might seem to contradict results from simulations (Hernquist 1989; Moreno et al. 2015), that suggest a central burst of star formation can occur in a galaxy after a close encounter with a companion if gas is present. However, our measurement of P_{gc} is susceptible to systematic uncertainties imposed by projection effects when estimating the separation between two galaxies. The effect of projection will be to increase our estimate of the tidal interaction strength, and as such each measurement is at best an upper limit. A further shortcoming of this technique results from the fact that there is a delay between the time of closest approach for two systems and the time at which nuclear star formation will be triggered and is able to be measured. This delay, and the inability to distinguish between systems infalling towards an interaction and those that are moving away after an interaction, makes identifying the signatures of tidal interactions difficult with this technique. Therefore, we cannot rule out the possibility that tidal interactions cause quenching in high-mass galaxy groups or enhancement in low-mass groups.

4.3.2 Projected phase-space

Within groups with halo mass greater than $10^{12.5}\,M_\odot$, we find no significant projected phase-space trends with $r_{50,\mathrm{H}\alpha}/r_{50,cont}$. Galaxies with the most centrally-concentrated star formation are predominantly found within r_{200}, with their group-centric distance distribution not differing significantly from other star-forming galaxies. With the exception of two systems their line-of-sight velocities relative to the group systemic velocity also lie mostly below the group velocity dispersion. Again, there is no significant difference between the distribution of line-of-sight velocities for galaxies with centrally concentrated star-forming galaxies and other star-formers. If rapid ram pressure stripping was responsible for the cessation of star formation in these galaxies soon after their infall into these massive groups we would expect a greater separation of these two types of galaxies in projected phase-space. Jaffé et al. (2015) observes the 21 cm neutral hydrogen emission line in galaxies outside the virialised region of galaxy clusters, and does not detect this line for galaxies that have presumably resided in clusters for some time. Given the difference in halo mass between the groups in our sample and the cluster studied by Jaffé et al. (2015) it is difficult to draw direct comparisons, but it seems probable that many of the galaxies with centrally concentrated star formation are not on their first passage into their host groups. Indeed, comparing the distribution of these galaxies to the simulations of projected phase-space performed by Oman et al. (2013), we can conclude that the majority of centrally-concentrated star-forming galaxies have been in their groups for perhaps over three Gyr (see Oman et al. 2013, Figure 4). We interpret the distribution of these galaxies in projected phase space as a sign that the quenching of star formation by this outside-in mechanism is not instantaneous and persists over several group-crossing times.

4.4 Comparison to other work

Our results have built on the work presented in Schaefer et al. (2017), and we find general agreement with the trends presented therein. While our previous work compared the spatial extent of star formation to the fifth-nearest neighbour surface density environment measure, the use of galaxy group properties has provided a framework for a more physical understanding of the processes at play. In contrast to Schaefer et al. (2017), we do find an anti-correlation between the scale-radius ratio and the stellar mass of the galaxies,

but this is only observed in more massive group haloes. The quenching of galaxies with stellar mass greater than $10^{10}\,M_\odot$ from the outside-in in dense environments is consistent with our previous findings, with the lack of this signature at lower stellar masses made more significant by our expanded sample.

These results from SAMI echo the findings from Hα narrow-band imaging presented in Kulkarni (2015). Kulkarni observed that galaxies with small scale-radius ratios lie below the star formation main sequence. The centrally-confined distribution of star formation in these galaxies, along with an observed upturn in the stellar light profiles in the outskirts of the galaxies led them to conclude that a combination of ram pressure stripping and gravitational interactions are the primary mechanisms influencing group galaxies today. While with SAMI we are unable to investigate the outer stellar discs of our sample, we do find agreement in the star formation morphologies. A future study that combines the radial coverage of narrow-band imaging with the spectroscopic advantages of integral field surveys will yield important clues as to the relative impact of these two processes on shaping the galaxy populations of today.

Bekki (2014) produced hydrodynamical simulations of the ram pressure stripping of gas from galaxies in groups and clusters. With these simulations they showed that the scale size of the star-forming discs of galaxies under ram pressure stripping can be reduced by a factor of two or more, depending on the halo mass of the group. In these simulations, galaxies under the influence of ram pressure stripping were capable of having their star formation either enhanced or suppressed. For satellite galaxies ($M_* > 10^{10}\,M_\odot$) in our massive group sample, a reduction in the scale size of the star-forming disc is always accompanied by a reduction in the total specific star-formation rate. The galaxies for which we do see a reduced scale radius ratio accompanied by an enhancement of the integrated star formation rate are the centrals of low-mass group halos and are unlikely to be undergoing ram pressure stripping and perhaps more likely to have undergone recent minor mergers or experienced fuelling from extragalactic gas (Janowiecki et al. 2017).

In Figure 4 we showed that galaxies in massive groups ($M_H > 10^{12.5}$) with stellar mass greater than $10^{10.1}\,M_\odot$ display a different star formation morphology as they become quenched than galaxies with lower stellar mass. Galaxies with lower stellar mass tend to quench with a more spatially extended star-formation morphology. The difference in the qualitative signatures of quenching at different stellar masses is difficult to reconcile with the idea of ram pressure stripping being the primary quenching mechanism for all galaxies. Bekki et al. (2002) showed that the removal of the halo gas surrounding a spiral galaxy resulting in the strangulation of the gas supply to the disc will result in the formation of an anaemic spiral. These simulations showed that as an anaemic spiral is formed, the star formation will fade uniformly across the galaxy disc. This may suggest that the quenching of star formation in galaxies with stellar mass less than $10^{10}\,M_\odot$ is caused by strangulation. This is a conclusion reached independently by Davies et al. (2016a), who observed that the rate at which low mass satellite galaxies become passive is consistent with the mechanism being strangulation.

5 CONCLUSION

We have used data from the SAMI Galaxy Survey to study the processes that suppress star formation in groups identified in the GAMA Galaxy Group Catalogue. The GAMA data provided several different metrics by which to quantify the environments of the galaxies in our sample. Our analysis shows that the dynamical mass of the group is a good predictor for the environmental quenching of star formation in galaxies of all stellar masses, with environmental quenching being strongest in groups more massive than $10^{12.5}\,M_\odot$. The tidal interaction parameter presented in Equation 4 does not correlate with any measurement of star formation suppression or enhancement, ruling out rapid quenching by tidal interactions. We also showed that the positions of quenching galaxies in their group projected phase-space are inconsistent with ram pressure stripping acting on their first passage through the group. The quenching of star formation in galaxy groups must take longer than the group dynamical time.

The spatial signature of this quenching appears to depend on the stellar mass of the galaxies. We find that for galaxies with stellar masses above approximately $10^{10}\,M_\odot$ in high-mass groups the scale radius of the star formation is reduced relative to that of the continuum for $29^{+8}_{-7}\%$ of galaxies, compared to $4^{+3}_{-4}\%$ for similar galaxies that are not in groups. This central confinement of the star formation is also associated with a reduction in the total star formation, with no strong evidence for central enhancement of star-formation. In the same groups, and in galaxies with stellar masses less than $10^{10}\,M_\odot$, the suppression of star formation does not show a tendency to accompany a central concentration of star formation. The qualitative variation in the spatial signature of quenching as a function of stellar mass suggests that different mechanisms are at play. Low-mass systems maintaining spatially-extended star formation while they become quiescent is consistent these galaxies quenching through strangulation, as was concluded by Davies et al. (2016a). In satellite galaxies in massive groups with stellar masses greater than $10^{10}\,M_\odot$, the central confinement of star formation during the transition from star-forming to quiescent is more consistent with ram-pressure stripping, tidal interactions, or a combination of both, taking place over several Gyr to quench star formation. This conclusion is in agreement with the simulations of Bekki (2014) and the estimated timescales is broadly consistent with the environmental quenching timescales outside of groups derived by other surveys (Rasmussen et al. 2012; Fossati et al. 2017).

REFERENCES

Abazajian K. N., et al., 2009, ApJS, 182, 543-558
Allen J. T., et al., 2015, MNRAS, 446, 1567
Alpaslan, M., Driver, S., Robotham, A. S. G., et al. 2015, MNRAS, 451, 3249
Baldwin J. A., Phillips M. M., Terlevich R., 1981, PASP, 93, 5
Balogh M. L., Baldry I. K., Nichol R., Miller C., Bower R., Glazebrook K., 2004, ApJ, 615, L101
Bekki, K., Couch, W. J., & Shioya, Y. 2002, ApJ, 577, 651
Bekki, K. 2014, MNRAS, 438, 444
Boselli, A., & Gavazzi, G. 2006, PASP, 118, 517
Brown, T., Catinella, B., Cortese, L., et al. 2017, MNRAS, 466, 1275

Bryant J. J., et al., 2015, MNRAS, 447, 2857
Byrd G., Valtonen M., 1990, ApJ, 350, 89
Calzetti D., 2001, PASP, 113, 1449
Cappellari M., Emsellem E., 2004, PASP, 116, 138
Cardelli J. A., Clayton G. C., Mathis J. S., 1989, ApJ, 345, 245
Chabrier G., 2003, PASP, 115, 763
Colless M., et al., 2001, MNRAS, 328, 1039
Cortese L., et al., 2012, A&A, 544, A101
Croom S., Saunders W., Heald R., 2004, AAONw, 106, 12
Croom S. M., et al., 2012, MNRAS, 421, 872
Dahari O., 1984, AJ, 89, 966
Davies L. J. M., et al., 2015, MNRAS, 452, 616
Davies, L. J. M., Robotham, A. S. G., Driver, S. P., et al. 2016a, MNRAS, 455, 4013
Davies, L. J. M., Driver, S. P., Robotham, A. S. G., et al. 2016b, MNRAS, 461, 458
Driver S. P., et al., 2011, MNRAS, 413, 971
Eke V. R., et al., 2004, MNRAS, 348, 866
Finn, R. A., Zaritsky, D., McCarthy, D. W., Jr., et al. 2005, ApJ, 630, 206
Fossati, M., Gavazzi, G., Savorgnan, G., et al. 2013, A&A, 553, A91
Fossati, M., Wilman, D. J., Mendel, J. T., et al. 2017, ApJ, 835, 153
Geha M., Blanton M. R., Yan R., Tinker J. L., 2012, ApJ, 757, 85
Gunn J. E., Gott J. R., III, 1972, ApJ, 176, 1
Hernquist L., 1989, Natur, 340, 687
Ho I.-T., et al., 2016, Ap&SS, 361, 280
Hopkins A. M., et al., 2013, MNRAS, 430, 2047
Jaffé Y. L., Smith R., Candlish G. N., Poggianti B. M., Sheen Y.-K., Verheijen M. A. W., 2015, MNRAS, 448, 1715
Janowiecki, S., Catinella, B., Cortese, L., et al. 2017, MNRAS, 466, 4795
Kauffmann G., et al., 2003, MNRAS, 341, 54
Kauffmann G., et al., 2003, MNRAS, 346, 1055
Kennicutt R. C., Jr., 1998, ApJ, 498, 541
Kelvin L. S., et al., 2012, MNRAS, 421, 1007
Kewley L. J., Dopita M. A., Sutherland R. S., Heisler C. A., Trevena J., 2001, ApJ, 556, 121
Koopmann R. A., Kenney J. D. P., 2004, ApJ, 613, 851
Koopmann R. A., Kenney J. D. P., 2004, ApJ, 613, 866
Koopmann R. A., Haynes M. P., Catinella B., 2006, AJ, 131, 716
Kulkarni S., 2015, PhD Thesis, Ludwig-Maximilians-Universität
Larson R. B., Tinsley B. M., Caldwell C. N., 1980, ApJ, 237, 692
Liske J., et al., 2015, MNRAS, 452, 2087
Markwardt C. B., 2009, ASPC, 411, 251
Moreno J., Torrey P., Ellison S. L., Patton D. R., Bluck A. F. L., Bansal G., Hernquist L., 2015, MNRAS, 448, 1107
Oman, K. A., Hudson, M. J., & Behroozi, P. S. 2013, MNRAS, 431, 2307
Oman, K. A., & Hudson, M. J. 2016, MNRAS, 463, 3083
Owers, M. S., Allen, J. T., Baldry, I., et al. 2017, arXiv:1703.00997
Patton D. R., Torrey P., Ellison S. L., Mendel J. T., Scudder J. M., 2013, MNRAS, 433, L59
Peng Y.-j., et al., 2010, ApJ, 721, 193
Peng Y.-j., Lilly S. J., Renzini A., Carollo M., 2012, ApJ, 757, 4
Peng Y., Maiolino R., Cochrane R., 2015, Natur, 521, 192
Richards S. N., et al., 2016, MNRAS, 455, 2826
Robotham A. S. G., et al., 2011, MNRAS, 416, 2640
Robotham, A. S. G., Driver, S. P., Davies, L. J. M., et al. 2014, MNRAS, 444, 3986
Rasmussen J., Mulchaey J. S., Bai L., Ponman T. J., Raychaudhury S., Dariush A., 2012, ApJ, 757, 122
Schaefer A. L., et al., 2017, MNRAS, 464, 121
Schawinski, K., Urry, C. M., Simmons, B. D., et al. 2014, MNRAS, 440, 889
Sharp R., et al., 2015, MNRAS, 446, 1551
Taylor E. N., et al., 2011, MNRAS, 418, 1587
Tonry J. L., Blakeslee J. P., Ajhar E. A., Dressler A., 2000, ApJ, 530, 625
Vazdekis A., Sánchez-Blázquez P., Falcón-Barroso J., Cenarro A. J., Beasley M. A., Cardiel N., Gorgas J., Peletier R. F., 2010, MNRAS, 404, 1639
van de Sande, J., Bland-Hawthorn, J., Fogarty, L. M. R., et al. 2017, ApJ, 835, 104
von der Linden A., Wild V., Kauffmann G., White S. D. M., Weinmann S., 2010, MNRAS, 404, 1231
Wijesinghe D. B., et al., 2011, MNRAS, 410, 2291
Wilman D. J., et al., 2005, MNRAS, 358, 88
Yang, X., Mo, H. J., van den Bosch, F. C., et al. 2007, ApJ, 671, 153
York D. G., et al., 2000, AJ, 120, 1579